doi.org/10.1002/batt.202000078



Special Collection

# A Novel $Li^+$-Conducting Polymer Membrane Gelled by Fluorine-Free Electrolyte Solutions for Li-Ion Batteries

Maria Assunta Navarra,*[a] Akiko Tsurumaki,[a] Francesco Maria Vitucci,[b] Annalisa Paolone,[b] Oriele Palumbo,[b] and Stefania Panero[a]

Gel polymer electrolytes (GPEs), composed of poly(vinylidene fluoride) (PVdF), a ternary solvent of ethylene carbonate:propylene carbonate:dimethyl carbonate, and LiBOB, which are characterized by a novel composition with a fluorine-free lithium salt, are here proposed. GPEs were firstly prepared through a solution casting procedure using the ternary carbonate solution as a solvent (named *ex situ* prepared membranes), and then activated by being immersed in a 0.7 M LiBOB-carbonate solution. Fundamental characterizations, including thermal, spectroscopical, mechanical, and electrochemical analyses, were carried out and compared before and after the activation. GPEs, having the same composition, were also prepared by using a novel procedure (named *in situ* prepared membranes), involving the formation of PVdF membrane and its activation by the LiBOB electrolyte, as well as subsequent electrochemical characterizations, in the same T-shape cell. Thus prepared lithium-ion batteries, employing Sn–C and $LiFePO_4$ electrodes, were demonstrated to exhibit a high capacity of 150 mAh $g^{-1}$ through the course of cycling.

## 1. Introduction

Lithium-ion batteries are currently the energy storage device of choice for the consumer electronic market. Moreover, they are gathering great attention because of their outstanding applications such as storage systems for renewable energy plants (REPs), as well as power sources for low-emission hybrid electric vehicles (HEVs) and even for emissions-free fully electric vehicles (EVs).[1] However, safety issues associated with conventional electrolytes based on organic carbonates and $LiPF_6$, such as flammability and formation of corrosive gas, are still preventing an expansion of this electrochemical technology.[2]

Many approaches have been proposed to suppress flammability of carbonate solvents using organic flame-retardants or additive salts (including ionic liquids).[3] Traditionally, they had low concentration, but in recent years, mixtures with high additive concentration are also being used.[4] In addition, solid-type electrolytes based on polymer matrices,[5] inorganic ceramics,[6] and plastic salts[7] have been reported as non-flammable electrolytes. It is well known that improvements in terms of safety and also reliability can be achieved by shifting from liquid solutions to solid electrolytes.[8] Despite of many favorable properties related to the nature of solid state, including negligible electrolyte leakage, practical use of all-solid-state lithium battery is still limited due to low room temperature ionic conductivity of the solid electrolytes and/or a coarse interface between the electrolyte and electrodes. Gel polymer electrolytes (GPEs), formed by a polymer matrix soaking a liquid electrolyte, present attractive features, since they have combined advantage of mechanical and chemical stabilities of polymer, as well as good ionic conductivity of liquid.[9] Poly(vinylidenefluoride) (PVdF) has been acknowledged as a potential polymer matrix because of its high resistivity against chemical, thermal, and electrochemical stresses, which is reinforced by the C–F bonds having a high biding energy.[10] In addition, many copolymers such as poly(vinylidene fluoride-co-hexafluoropropylene) (PVdF-HFP)[11] and poly(vinylidene fluoride)/polymethacrylate[12] have been developed as a matrix for GPEs.

With respect to the components in the liquid electrolyte, $LiPF_6$ is acknowledged as one of the potential salts for lithium-ion batteries because of its good ionic conductivity and negligible reactivity toward aluminum current collectors.[13] However, several drawbacks of $LiPF_6$ salt are widely known in literature, such as an unavoidable formation of HF caused by a trace amount of moisture.[14] This is owing to relatively unstable P–F bonds, unlike C–F bonds found in polymers. To overcome this problem, the substitution of highly reactive $LiPF_6$ with more stable fluorine-free salts was considered.[15] Among new electrolyte salts, lithium bis(oxalato)borate (LiBOB) is a very promising candidate because of its attractive properties, such as a high thermal stability, the ability to stabilize solid electrolyte interphase (SEI), and the addition of overcharge tolerance to electrodes.[14a,15a,16] Chen *et al.* demonstrated that, capacity retention of graphite|$LiMn_{1/3}Ni_{1/3}Co_{1/3}O_2$ cells, having $LiPF_6$/LiBOB blend salt-based electrolyte, increases with the LiBOB

[a] Dr. M. A. Navarra, Dr. A. Tsurumaki, Prof. S. Panero
Department of Chemistry
Sapienza University of Rome
Piazzale Aldo Moro 5, 00185 Rome, Italy
E-mail: mariassunta.navarra@uniroma1.it
[b] Dr. F. M. Vitucci, Dr. A. Paolone, Dr. O. Palumbo
CNR-ISC, U.O.S.
Sapienza University of Rome
Piazzale Aldo Moro 5, 00185 Rome, Italy

Supporting information for this article is available on the WWW under https://doi.org/10.1002/batt.202000078

Special Collection *An invited contribution to a Special Collection on Electrolytes for Electrochemical Energy Storage*

concentration. In addition, a $LiPF_6$-free composition, particularly 0.7 M LiBOB in ethylene carbonate:propylene carbonate:dimethyl carbonate (EC:PC:DMC) 1:1:3 by weight, showed good capacity retention at 55 °C.[17] Hassoun *et al.* demonstrated that the same solution exhibits promising performances in a complete lithium-ion cell formed by partially pre-lithiated Sn–C anode and $LiFePO_4$ cathode.[18] They also prepared GPEs using the same solution and demonstrated their good cycling performances in $SnC/LiFe_{0.5}Mn_{0.5}PO_4$, specifically 100 mAh $g^{-1}$ throughout 70 cycles.[19]

Herein, we present GPEs composed of 0.7 M LiBOB in EC:PC:DMC 1:1:3 by weight and PVdF prepared through both *ex situ* and *in situ* procedures. In general, the synthesis of *ex situ* GPEs consists of preparing a dry membrane, cutting into a cell dimension, and swelling in a liquid electrolyte.[12] In addition, after cell assembling, it is recommended to age the cells for few days to allow wetting of the electrodes by electrolyte.[21] In contrast, *in situ* GPE can be prepared directly between electrodes in a prototype cell. The *in situ* GPE not only simplifies the preparation but also improve an interfacial contact between the electrodes and the electrolyte.[22] Also, *in situ* gels are effective for a suppression of dendric lithium formation.[23]

The GPE and its individual components were characterized in terms of thermal properties, spectroscopic properties, and mechanical behavior. Electrochemical characterization was performed in terms of temperature-dependent ionic conductivity, electrochemical stability window, stability at the interface both with lithium metal and Sn–C electrodes, as well as galvanostatic cycling in half cells with $LiFePO_4$ and Sn–C electrodes. The GPE was finally tested in a full Sn–C/LiFePO4 lithium-ion cell.

## 2. Results and Discussion

GPEs have been prepared according to two different procedures (Figure 1). For the purpose of fundamental characterization, GPEs were prepared by a traditional solution casting procedure using the ternary carbonate mixture as a solvent.

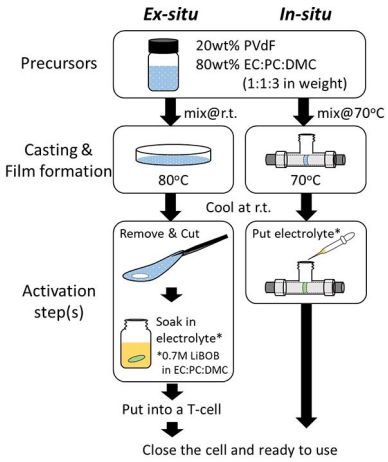


**Figure 1.** *Ex situ* and *in situ* procedure of PVdF-based GPE preparation.

The thus prepared systems (named *ex situ* membrane), having the appearance of transparent, self-standing and flexible membranes with good film-forming ability, were activated by using 0.7 M LiBOB solution.

Figure 2 shows the results of differential scanning calorimetry (DSC) of *ex situ* membranes, both in pristine and activated state. Thermal transitions of the pristine membrane, related to the crystallization of carbonates,[24] are almost suppressed upon the activation in 0.7 M LiBOB EC:PC:DMC. The activated sample does not show any crystallization/melting transition; in particular, the endo-thermic melting process around 0 °C disappears upon activation, which is favorable for low temperature applications since the crystallization causes conductivity to plummet.[4c] Only a glass transition is observed around −85 °C in the activated sample. This finding indicates the expansion of applicability, especially at low temperatures, for this particular composition.

The thermogravimetric analysis (TGA) curve of the activated membrane is reported as a red line in Figure 3, and that of the pristine membrane is also reported as a blue line. For a comparison, the TGA has been carried out also for the initial PVdF and LiBOB powders (black and green lines, respectively).

The initial PVdF is found to be highly stable up to 430 °C, in close agreement with results reported in the literature.[25] Decomposition of LiBOB salt starts at lower temperatures about 300 °C and 480 °C by a two-step process. It is known indeed that in the first stage LiBOB decomposes into lithium oxalate ($Li_2C_2O_4$), boron oxide glass ($B_2O_3$), and $CO_x$ gases, and

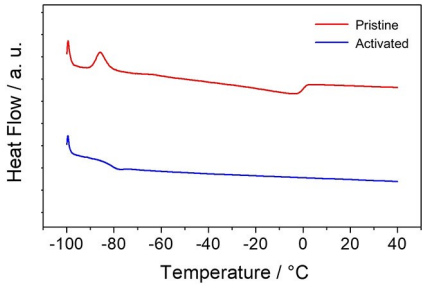


**Figure 2.** DSC traces of *ex situ* prepared pristine and activated GPEs.

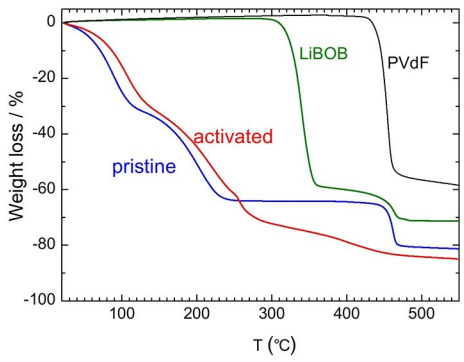


**Figure 3.** TGA curves of PVdF powder (black) and LiBOB powder (green), as well as *ex situ* prepared pristine membrane (blue), and GPE activated in EC:PC:DMC 0.7 M LiBOB (red).

subsequently the former two solid products react and transform into lithium triborate ($LiB_3O_5$).[26] The thermal stability of this non-fluorinated salt is highly advantageous in terms of safety and reliability, especially if it is compared to the limited stability of $LiPF_6$ (*i.e.* below ca. 100 °C).

In the case of pristine *ex situ* membrane (blue line), the mass losses below 200 °C are caused by the multi-step removal of the volatile solvents, while the mass loss above 400 °C is due to the decomposition of the PVdF matrix, which is in accordance with the thermal decomposition temperature of the initial powder.

The removal of solvents is also detectable in the curve of the activated *ex situ* membrane (red line). However, in this case, the mass losses slightly shifted to higher temperatures as compared to the pristine one, indicating a small improvement in thermal stability with the addition of LiBOB. The behavior of the mass loss above 250 °C, which is considered to relate to the decomposition of the PVdF and LiBOB components, is rather different than both the traces measured for the pure PVdF, LiBOB and pristine membrane, as it does not exhibit any plateau but had gradual sloping pattern upon heating. The change in the curve shape suggests enhanced interactions among the components which alter the properties of the membranes.

In order to obtain more information about the interactions, the samples have been studied by means of vibrational spectroscopy (Figure 4). In particular, to investigate the temperature dependence of the infrared (IR) spectra, we heated several pieces of the activated GPE up to selected temperatures

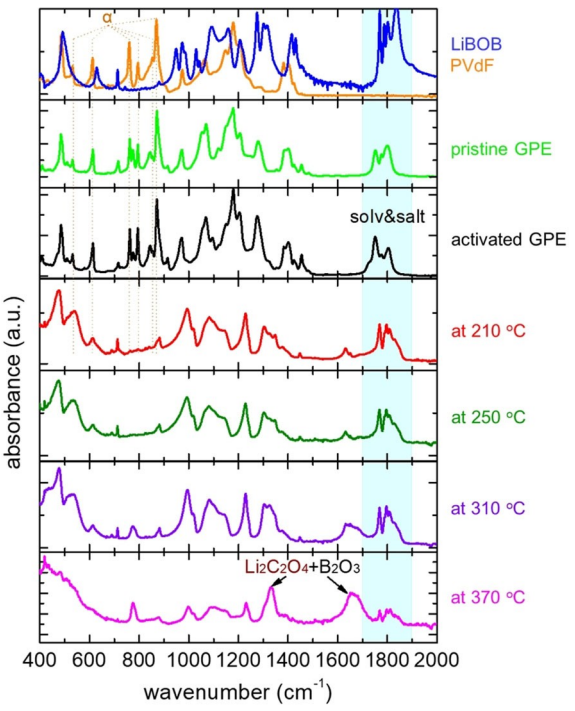


**Figure 4.** IR spectra collected at room temperature for pure PVdF (orange), pure LiBOB (blue), pristine GPE (light green), activated GPE (black), and the activated GPE after treatment at 210 °C (red), 250 °C (dark green), 310 °C (violet) and 370 °C (pink).

(210, 250, 310 and 370 °C) at a constant rate of 4 °C min$^{-1}$ in an argon flux of 40 ml min$^{-1}$. The IR spectra of these thermally treated membranes were collected at room temperature. For a comparison, the spectra measured for pure PVdF and LiBOB powders are also reported in Figure 4.

In the IR spectra of both pristine (containing solely EC:PC:DMC) and activated (containing 0.7 M LiBOB in EC:PC:DMC) membranes, bands assigned to the carbonates were found at 775 cm$^{-1}$ ($CO_3$ non-planar rock), 1179 cm$^{-1}$ ($CO_2$ sym. stretch), 1279 cm$^{-1}$ ($CO_2$ sym. stretch), and 1454 cm$^{-1}$ (C–O asym. stretch), as well as between 1700 and 1900 cm$^{-1}$ (C=O stretching mode).[27] In the latter case, a superposition of bands of the PVdF and the LiBOB electrolyte solution was found between 900 and 1500 cm$^{-1}$, as it is obvious in the spectra of starting pure materials. Only in the region below 900 cm$^{-1}$, it is possible to distinguish several absorption bands of PVdF (531, 612, 766, 795, 855 and 873 cm$^{-1}$), which are characteristic signals of its $\alpha$-phase structure having a non-polar TGTG conformation.[28] More in detail, the band at 795 cm$^{-1}$ is attributed to a combination of the $CH_2$ rocking and $CF_3$ stretching modes, and the band at 873 cm$^{-1}$ is assigned to a combination of CC symmetric stretch and CCC deformation in PVdF.[28b] The other superposition of bands was observed between 1700 and 1900 cm$^{-1}$ related to LiBOB and carbonate solvents.

In contrast to the room temperature samples, the heated samples display less structured patterns, as many features disappear and broaden. In particular, in the spectrum of the sample heated up to 210 °C, the bands from the solvents such as those at around 1279 and 1454 cm$^{-1}$ disappear, while the signals between 1700 and 1900 cm$^{-1}$ change their shape but are still present. The altered peaks are assigned to LiBOB, specifically 1768 and 1796 cm$^{-1}$ (C=O stretching), 1808$^{-1}$ (free BOB-), as well as 1810 and 1828 cm$^{-1}$ (Li coordinated BOB-).[29] The shoulder around 1820 cm$^{-1}$ is visible only in the spectra of the thermally treated samples. This confirms that LiBOB is effectively dissociated in the room temperature samples because of the presence of the carbonates. In the spectra of the thermally treated samples, the bands of the $\alpha$-phase PVdF are no more detectable, while new signals appeared (specifically at 882 and 1082 cm$^{-1}$), that are assigned to the polar TTGG conformation of $\beta$-phase PVdF.[28a,c] This suggests that during the heating treatment of samples, a rearrangement in the crystalline phase of PVdF (from $\alpha$ to $\beta$ phase) occurs, and a part of the samples possibly becomes amorphous as represented by the broaden bands of the heated samples. Indeed, the conversion of the crystalline phase in PVdF has already been observed upon hot-stretching[28a] or polarization.[30] The formation of $\beta$ phase was also observed in the IR spectra of the pristine membranes after heating treatments (See Figure S1 in the ESI). However, in this case, the presence of the $\beta$ phase was observed not at 210 °C but at 370 °C; the transition temperatures shifted towards higher values. This is probably due to the absence of interactions between the PVdF and the lithium salt. With respect to the structure of LiBOB, two new lines at around 1350 and 1650 cm$^{-1}$ were observed by the heating

treatment, which are assigned to $Li_2C_2O_4$ formed through the decomposition of LiBOB (see Figure S2 in the ESI).

The results obtained from IR analysis indicate that the components in the activated GPE, *i.e.* PVdF and the LiBOB solution, deeply interact, and the interactions seem to positively affect the increase in the boiling temperatures of the electrolyte but caused a decrease in the decomposition temperature of the polymer (see Figure 2), of which the former has stronger implications for practical use because of its proximity to the desired applicability temperature range.

The storage modulus and the energy dissipation of the *ex situ* membranes in pristine and activated state between 30 °C and −100 °C are reported in Figure 5 (upper and lower panel, respectively).

During the first cooling (circle plots), the pristine membrane shows an abrupt increase of the modulus around −50 °C and a peak in the elastic energy dissipation with the maximum at −75 °C for a vibration frequency of about 10 Hz. On heating back to room temperature (triangle plots), E′ and tan δ present the same features observed in the cooling scan but with a large hysteresis, as the modulus abrupt change is found between −20 and 5 °C and as the peak in tan δ is detected around −50 °C. The peak corresponds to glass transition, the temperature of which is in agreement with the results of DSC analysis, and the change in modulus is considered to be related to the melting feature of the carbonate mixture, which is observed as a broad endothermic peak in DSC. The values measured at room temperature for the two physical properties are the same between heating and cooling scans (E′ around $3\times10^6$ Pa; tan δ about 0.17).

In the cooling scan of the activated membrane (open circles in the lower panel of Figure 5), the storage modulus and the tan δ present the features similar to those of the pristine membrane, but temperatures inducing all phenomena shifted to lower values. Specifically, the abrupt increase of the modulus is detected about −70 °C and the accompanying peak in tan δ is at about −80 °C for a vibration frequency of about 10 Hz. These temperature values are close to the thermal process revealed by DSC analysis, indicating that the change in the storage modulus can be ascribed to the glass transition. Moreover, it can be noted that the modulus values of the activated membrane (about $2\times10^7$ Pa at room temperature) are considerably higher than that of the pristine membrane, indicating a reinforcing effect by LiBOB. The measurements carried out by heating the activated membrane (open triangles) show the modulus curve identical to the cooling curve. The large hysteresis observed in the pristine membrane is thus drastically reduced upon the addition of the Li salt, denoting better mechanical stability of the activated membrane. In addition, the curve of subsequent cooling scan is almost coincident with the curves of the first cycle, confirming the good mechanical stability upon thermal cycling.

The Arrhenius plot of conductivity for the *ex situ* prepared membrane activated in the 0.7 M LiBOB electrolyte is reported in Figure 6. Of particular interest is the fact that the GPE here investigated shows high, temperature-enhanced conductivity values. Specifically, this particular GPE composition exhibited a conductivity approaching $10^{-3}$ S cm$^{-1}$ at the room temperature, which is comparable to the value of some liquid electrolytes,[31] and it retained the value of $10^{-4}$ S cm$^{-1}$ even at −20 °C. Taking into account the facts that the explored temperature is low and the film is in a solid-like state, this conductivity value is considered to be sufficiently high. The good conductivity is in agreement with the low glass transition temperature (−85 °C) measured by DSC. Note that general polymer electrolytes usually display a conductivity decrease due to the drop in the low temperature range due to the occurrence of crystallization phenomena of polymers.

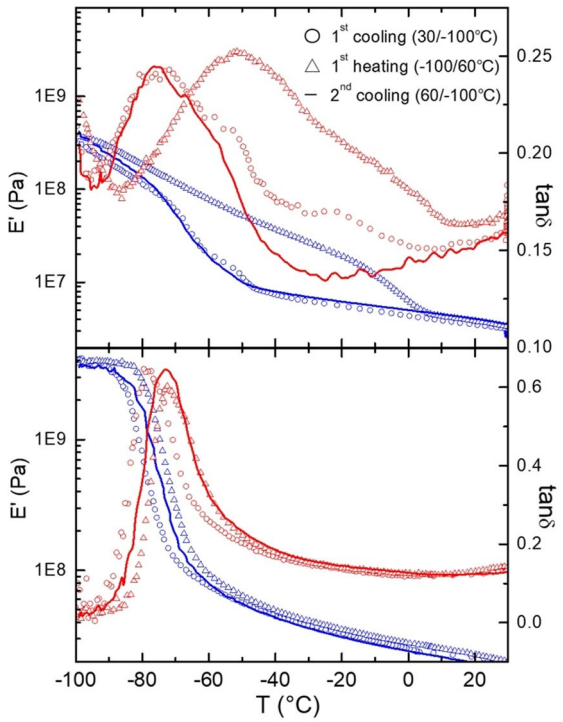


**Figure 5.** Storage modulus (E′, blue) and elastic energy dissipation (tan δ, red) of the pristine membrane (upper panel) and the activated membrane (lower panel). Circle plots denote first cooling from 30 to −100 °C, triangle plots are for subsequent heating from −100 to 60 °C, and lines designate final cooling from 60 to −100 °C.

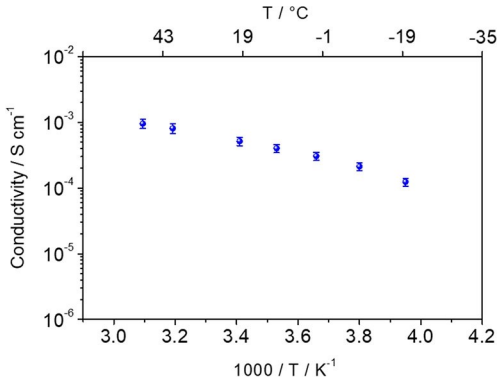


**Figure 6.** Arrhenius plot of the ionic conductivity of the *ex situ* prepared, activated membrane.

The temperature dependency of conductivity was adequately fitted using the Vogel-Tammann-Fulcher (VTF) equation rather than using the Arrhenius equation. This means the conductivity is also affected by segmental relaxation in GPE. The VTF equation is as follows:

$$\sigma_i = \frac{A_\sigma}{\sqrt{T}} \exp\left(\frac{-B_\sigma}{T - T_0}\right) \quad (1)$$

in which, $\sigma_i$ is the measured conductivity, $T$ is the temperature for the measurement, while $T_0$, $B_\sigma$, and $A_\sigma$ are the fitting parameters. In this study, $T_0$ was defined as $T_g$ −50 °C. The activation energy for ion conduction ($E_a$) was calculated by multiplying the slope of VTF fitting, *i.e.* $B_\sigma$, with the gas constant. The $E_a$ of GPE was found to be 5.4 kJ mol$^{-1}$. The value is slightly higher compared to that of poly(acrylonitrile)-based GPE (2.5 kJ mol$^{-1}$)[32] and of poly(vinylacetate)-based GPE (0.05 eV).[33]

The electrochemical stability window (ESW) versus carbon-based electrodes was investigated by linear and cyclic voltammetries in anodic and cathodic regions, respectively (Figure 7). The membrane activated in the LiBOB solution exhibits a peak at around 1.7 V vs Li$^+$/Li, which is the typical reduction peak of borate anions on carbon.[3b] This peak disappears in subsequent cathodic cycles because of a formation of a SEI during the first cycle, which stabilizes the anode-electrolyte interface and prevents decompositions of electrolyte in the low-voltage range. The current flow between 1 V and 0.5 V vs Li$^+$/Li in the first cathodic scan is ascribed to a lithium deposition, which is probably accompanied by a slight decomposition of solvents. In the reverse scan, lithium de-intercalation takes place, resulting in the almost same current value upon cycling, which confirms a reproducible lithium intercalation/de-intercalation process. In the anodic side, an increase of current is detected at 5.0 V vs Li$^+$/Li. When an anodic scan of LiBOB-carbonate solution was measured using a glass fiber separator, the current peak was observed at 5.5 V.[3b] The lowered oxidation voltage is possibly caused by the enhanced interactions among the components as discussed in the former sections, or the presence of impurities, especially if we take into account the low current density.

The performance of the GPE in lithium metal half-cells and lithium-ion full cells were then evaluated. In addition, prior to evaluating the cell performances, the interfacial properties of *in situ* GPE on anode surfaces, such as Li and SnC, were analyzed. For these analysis *in situ* prepared membranes were used (see Figure 1), *i.e.* the membranes were prepared directly between a pair of selected electrodes and activated in the same T-shape cell.

Stability analysis *versus* time lapse was performed by recording the impedance spectra of the *in situ* prepared, activated membrane versus selected anodes (Figure 8). Resistances at the membrane/electrode interphase, given by the amplitude of the semicircles in impedance spectra, as well as the shape of the spectrum, drastically vary according to the nature of the interphase. As reported in literature, when liquid electrolytes are used, two semicircles were observed for SnC|SnC cells and one main semicircle was observed for Li|Li cells.[34] In the former case, the semicircles in a higher and lower frequency range are associated with a SEI resistance ($R_{SEI}$) and charge transfer resistance ($R_{ct}$), respectively. In our case, the feature associated to the low-frequency range was pronounced after 7 days and only a part of arc was observed. This is probably due to due to diffusion constrain on the Sn–C surface. An increase in the interfacial resistance with elapsed time is observed at the interphase with both Li and Sn–C electrodes. However, compared to a liquid electrolyte, the growth in resistance is much better controlled by using the proposed GPE. In addition, the bulk resistance was constant throughout the course of measurements. Moreover, compared to *ex situ* GPEs reported in literature, having similar composition, the interfacial resistance against Li was found to be smaller in the present study.[19] This proves the improved contact between

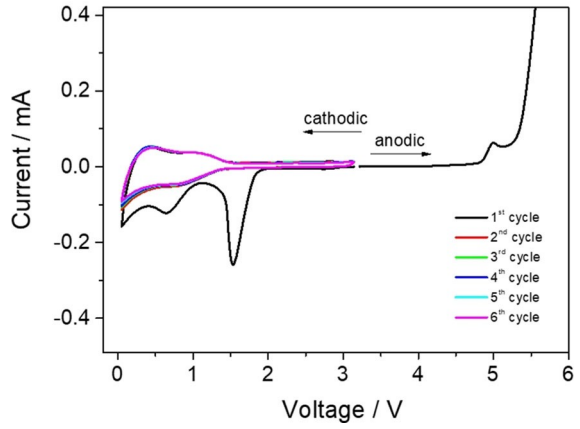


**Figure 7.** ESW of the *ex situ* prepared membrane in the activated state, measured by using super P carbon as a working and Li as a counter-reference electrode.

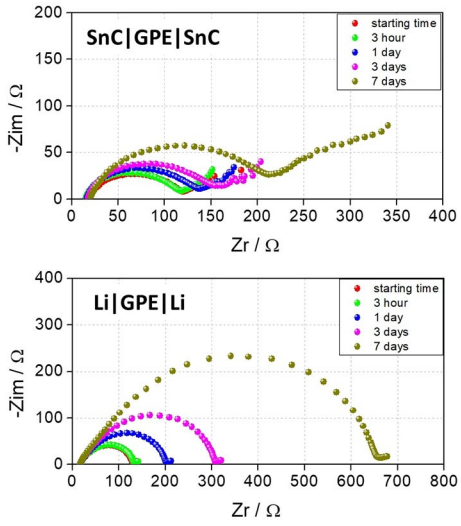


**Figure 8.** Nyquist plots of the impedance spectra of symmetric SnC|GPE|SnC (upper) and Li|GPE|Li (lower) cells, with the *in situ* prepared activated GPE, at open circuit voltages

the in situ GPE and Li by preparing the GPE directly between the electrodes. Overall, with both electrodes the GPE here proposed shows acceptable interfacial resistance values, proving a high compatibility of the selected membrane/electrode combinations.

The *in situ* prepared activated membrane was tested in lithium metal half-cells employing $LiFePO_4$ or Sn–C electrodes, which were chosen as potential electrode pair for possible Li-ion cell applications. Voltage profile *versus* specific capacity is reported in Figure 9. The cell having $Li|LiFePO_4$ composition exhibits a flat voltage profile, which is characteristic of olivine type materials, centered at around 3.5 V vs $Li^+/Li$. This is achieved solely when the electrolyte has sufficient conductivity. The overvoltage was around 0.3 V. This value is slightly higher than that of liquid cells.[19] However, such values are frequently observed and are acceptable for GPEs.[22,23] The high coulombic efficiency and very stable charge/discharge behavior were reproducible throughout 200 cycles. In the case of the cell with Sn–C, reversible capacity values about 280 mAh $g^{-1}$, arose from $Li^+$ alloying/de-alloying, are obtained after the first discharge process (Figure 9, lower panel). In this voltage range, the reductive decomposition of BOB anion is observed during the 1 $^{st}$ discharge at around 1.7 V vs $Li^+/Li$, which is in accordance to the ESW of the *ex situ* membranes. The decomposition together with the volume change of Sn–C caused the irreversible capacity during the 1$^{st}$ cycle. After the formation of SEI, the irreversible capacity was diminished with very good efficiency upon the following cycles. Both cell performances confirm that the pair of SnC anode and $LiFePO_4$ cathode are a good combination for a GPE-based lithium-ion cell.

Based on the promising performances in the lithium metal half-cells, the *in situ* prepared GPE was then used as an electrolyte for the SnC|GPE|LFP lithium-ion cell (Figure 10). The specific capacity was calculated based on the mass of $LiFePO_4$. The cell exhibited the capacity of 160 mAh $g^{-1}$ in the first charge-discharge cycle, which is corresponding to 94% of the specific capacity of $LiFePO_4$ and good capacity retention over 10 cycles, with high coulombic efficiency (>95%). Upon following charge-discharge (up to a total of 40 cycles), a good coulombic efficiency is retained (98.4% at 40$^{th}$ cycle) but a slow decay of the full-cell performances is observed. This is probably due to non-optimized operating conditions, such as cathode/anode balancing and voltage range. Even though this is just a preliminary attempt, it demonstrates that the GPE proposed here is suitable for $SnC|LiFePO_4$ lithium-ion cell composition. The *in situ* prepared GPEs were concluded to be a promising gel electrolyte which possesses high safety and good lithium-ion cell performance.

## 3. Conclusions

A novel GPE, based on PVdF and a ternary carbonate mixture dissolving 0.7 M LiBOB, prepared by using both *in situ* and *ex situ* procedures, is here proposed. In the former case, the gelation of PVdF and soaking of the LiBOB electrolyte was carried out in the T-shape cell used for electrochemical analyses, while in the latter case the PVdF membrane was prepared through general solution casting procedure with electrolyte soaking steps and following cell assembly. The fundamental properties were analyzed with respect to *ex situ* prepared GPE, confirming its promising features as GPE in terms of low glass transition temperature (*i.e.*, −85 °C without crystallization), high thermal and mechanical stability, synergistic interactions among components and wide electrochemical stability in the potential range of general lithium-ion batteries. The galvanostatic performance in lithium metal half-cells, i.e. Li|LFP and Li|SnC configurations, as well as in full Sn–C|LFP lithium-ion cells, were evaluated with respect to *in situ* prepared GPE. Most remarkably, the lithium-ion cells exhibited capacity values as high as 160 mAh $g^{-1}$.

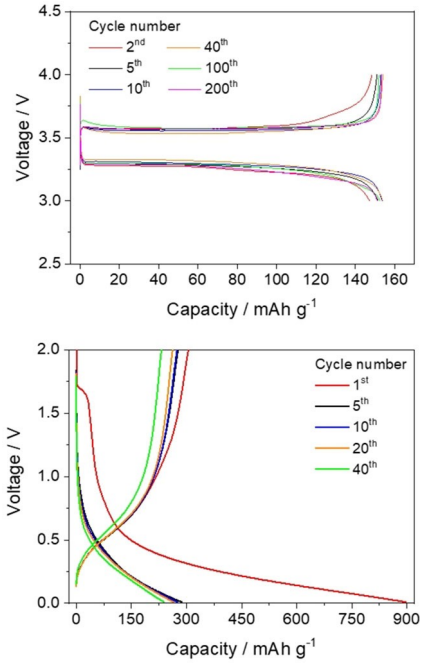


**Figure 9.** Voltage profiles during charge/discharge cycles of Li|GPE|$LiFePO_4$ (upper) and Li|GPE|SnC (lower) cells.

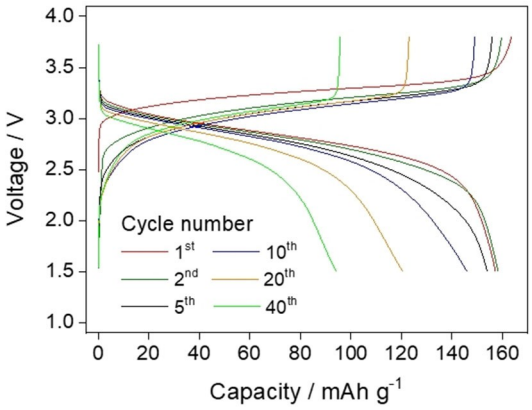


**Figure 10.** Voltage profiles of charge/discharge cycles of a SnC|GPE|$LiFePO_4$ lithium-ion cell.

## Experimental Section

### GPE preparations

PVdF (PVdF Solvay Solef 6020), EC (Merck), DMC (Merck), PC (Merck), and LiBOB (Chemetal) were purchased from each company and used without any further purification. Storage of the reagents and preparation of membranes were done in an Ar-filled glove box. Two different procedures, indicated as *ex situ* and *in situ*, have been applied for the membrane preparations (see Figure 1). Thus prepared pristine polymer membranes are activated by being immersed in the 0.7 M LiBOB liquid electrolyte.

*Ex situ* preparation consists of the synthesis of a self-standing stable membrane as a first step, specifically i) mixing PVdF with the selected organic solvent mixture (i.e. EC:PC:DMC) in the weight ratio of 20:80 at room temperature, ii) casting the resulting dispersion on a Petri dish at 80 °C, and iii) rapid cooling at room temperature. It should be noted that to avoid undesired removal of the volatile components and to keep the ratio among solvents and polymer constant, all steps are performed in closed containers (a vial for mixing and a Petri dish covered by stainless steel case for casting-cooling). Once the membrane is formed, the activation of membrane was carried out as a second step by immersing the membrane samples into the selected swelling solution (i.e. 0.7 M LiBOB in EC:PC:DMC) for 24 hours. Membranes with a thickness ranging between 200 μm and 300 μm are obtained.

*In situ* preparation is a procedure recently proposed by our group,[35] which is optimized according to the specific GPE composition in this study. This preparation is conveniently used to obtain a GPE directly in prototype cells for electrochemical measurements. Briefly, precursors of the membrane, having the composition described in Figure 1, were loaded and gelated in a T-shape cell between two electrodes, in the middle of which a Whatman disk was placed to avoid short circuits. Specifically, the polymer dispersion, described above (EC:PC:DMC/PVdF, 80/20 wt %) heated at 70 °C, was loaded into the cell at the same temperature. The cell was then cooled to room temperature. Subsequently, activation by lithium-salt infiltration was carried out by adding the swelling solution to the T-shape cell and by removing the solution in excess after 300 min.

Both GPE preparations were performed in a moisture-free atmosphere of an Ar-filled dry box having water content below 2 ppm.

### Characterizations

All the following physical-chemical characterizations were performed with respect to *ex situ* prepared GPEs, except for the evaluations of interfacial resistance and galvanostatic cycling. All the sampling procedures and the cell preparations were carried out in an Ar-filled glove box. The measurements were carried out at ambient atmosphere, unless particular conditions are mentioned.

Differential scanning calorimetry (DSC 821 Mettler-Toledo) measurements were performed under nitrogen flux, by cooling the samples to −100 °C at 4 °C min$^{-1}$, keeping at −100 °C for 10 min, and subsequently heating up to 40 °C at 4 °C min$^{-1}$. Only the heating scan will be here reported.

Thermo-gravimetry analyses (TGA) were carried out using a Setaram Setsys Evolution 1200 TGA System by heating the samples up to 600 °C at a constant rate of 4 °C min$^{-1}$ under argon flux of 40 ml min$^{-1}$.

The IR spectroscopy was performed using a Bruker Alpha spectrometer in the frequency range between 400 and 4000 cm$^{-1}$ with a resolution of 2 cm$^{-1}$. LiBOB samples were analyzed in transmission mode, by mixing their grinded powders with a KBr matrix in a weight ratio of ≈1/100. The spectra of PVdF powders and all the membranes were measured by using a diamond attenuated total reflectance (ATR) accessory. All measurements were conducted in an Ar-filled glove box in order to avoid contamination of water. All spectra were converted into absorbance data.

Dynamic mechanical analysis (DMA) was carried out using a Perkin-Elmer DMA8000 apparatus in tension mode. Sample membranes were cut into 4–6 mm width ×10–12 mm length. The storage modulus (E′) and the elastic energy loss (tanδ) were measured as a function of temperature in the range −100 °C ÷ 60 °C with a scan rate of 4 °C min$^{-1}$ at a frequency of 10 Hz. The DMA8000 was put into a glove bag filled with argon at dynamical pressure, following the procedure already reported in the literature.[36]

Temperature-dependent conductivity of the *ex situ* prepared GPE was measured by means of impedance spectroscopy using a potentiostat/galvanostat VSP Bio-Logic apparatus (10 mV amplitude signal, frequency range 200 kHz–1 Hz). Samples were housed in commercially available stainless steel coin-type cells, the cell constant of which was evaluated to be 0.04 cm$^{-1}$.

The electrochemical stability window of *ex situ* prepared GPE was determined based on linear sweep voltammetry and on cyclic voltammetry using a Perkin VMP potentiostat. The measurements were performed at a scan rate of 0.2 mV sec$^{-1}$, by using a T-shape cell having a Super P carbon-coated Al or Cu foil as the working electrode and lithium foil as the counter and reference electrode.

The stability of the interface between *in situ* prepared GPE and anode materials (*i.e.* Li and Sn–C) was evaluated by means of impedance spectroscopy recorded using a multichannel potentiostat/galvanostat analyzer VersaSTAT MC, Princeton Applied Research (PAR) (10 mV amplitude signal, in a frequency range of 100 kHz–0.1 Hz).

*In situ* GPE formed between either $LiFePO_4$/Li or Sn–C/Li was cycled galvanostatically by using a Maccor Series 4000 battery test system as a driving and controlling instrument. The 1$^{st}$ cycle of the $LiFePO_4$/GPE/Li cell was cycled at 170 mA g$^{-1}$, corresponding to 1 C, whereas the subsequent cycles up to the 200$^{th}$ cycle were recorded at 56.7 mA g$^{-1}$ (*i.e.* 0.33 C). The Sn–C/GPE/Li cell was cycled at 100 mA g$^{-1}$. Performance of a lithium-ion cell consisting of *in situ* GPE with Sn–C anode and $LiFePO_4$ cathode was also evaluated by means of galvanostatic cycles at 56.1 mA g$^{-1}$ in the voltage range 1.5–3.8 V vs $Li^+$/Li.

The Sn–C and $LiFePO_4$ electrodes used for analyses of interfacial stability and galvanostatic performances were prepared using doctor-blade deposition on a Cu and Al foil, respectively. The slurry having 80% of the active material, 10% of PVdF 6020, and 10% of Super P carbon was used. $LiFePO_4$ was a commercial product, while Sn–C was prepared in-house by the impregnation technique described in the literature.[37] To be noticed that, Sn–C electrodes were activated through *ex situ* lithiation prior to use.[9b]

## Acknowledgements

*M.A.N. acknowledges Sapienza University of Rome for funding the Project ELLIBAT "ELectrode active materials from end-of-life Lithium-ion BATteries" (Ateneo Research Project 2019, n. RM11916B863810FF). Daniele Di Lecce (University College London,*

*UK) and Jusef Hassoun (University of Ferrara, Italy) are gratefully acknowledged for fruitful discussions.*

## Conflict of Interest

The authors declare no conflict of interest.

**Keywords:** gel polymer electrolytes · energy storage · one-pot synthesis · lithium-ion batteries

[1] B. Scrosati, J. Garche, *J. Power Sources* **2010**, *195*, 2419–2430.
[2] a) K. Xu, *Chem. Rev.* **2004**, *104*, 4302–4417; b) S. Wilken, M. Treskow, J. Scheers, P. Johansson, P. Jacobsson, *RSC Adv.* **2013**, *3*, 16359.
[3] a) J. Kalhoff, G. G. Eshetu, D. Bresser, S. Passerini, *ChemSusChem* **2015**, *8*, 2154–2175; b) A. Tsurumaki, M. Branchi, A. Rigano, R. Poiana, S. Panero, M. A. Navarra, *Electrochim. Acta* **2019**, *315*, 17–23; c) T. Dagger, B. R. Rad, F. M. Schappacher, M. Winter, *Energy Technol.* **2018**, *6*, 2011–2022.
[4] a) Y. Yamada, J. Wang, S. Ko, E. Watanabe, A. Yamada, *Nat. Energy* **2019**; b) J. Wang, Y. Yamada, K. Sodeyama, E. Watanabe, K. Takada, Y. Tateyama, A. Yamada, *Nat. Energy* **2017**, *3*, 22–29; c) A. Tsurumaki, M. Agostini, R. Poiana, L. Lombardo, E. Lufrano, C. Simari, A. Matic, I. Nicotera, S. Panero, M. A. Navarra, *Electrochim. Acta* **2019**, *316*, 1–7; d) K. Ueno, K. Yoshida, M. Tsuchiya, N. Tachikawa, K. Dokko, M. Watanabe, *J. Phys. Chem. B* **2012**, *116*, 11323–11331.
[5] a) B. Scrosati, F. Croce, G. B. Appetecchi, L. Persi, *Nature* **1998**, *394*, 456–458; b) W. Zhou, Z. Wang, Y. Pu, Y. Li, S. Xin, X. Li, J. Chen, J. B. Goodenough, *Adv. Mater.* **2019**, *31*, e1805574.
[6] T. Hakari, M. Nagao, A. Hayashi, M. Tatsumisago, *J. Power Sources* **2015**, *293*, 721–725.
[7] D. R. MacFarlane, M. Forsyth, *Adv. Mater.* **2001**, *13*, 957–966.
[8] a) M. Marcinek, J. Syzdek, M. Marczewski, M. Piszcz, L. Niedzicki, M. Kalita, A. Plewa-Marczewska, A. Bitner, P. Wieczorek, T. Trzeciak, M. Kasprzyk, P. Łężak, Z. Zukowska, A. Zalewska, W. Wieczorek, *Solid State Ionics* **2015**, *276*, 107–126; b) J. Y. Song, Y. Y. Wang, C. C. Wan, *J. Power Sources* **1999**, *77*, 183–197.
[9] a) N.-S. Choi, Z. Chen, S. A. Freunberger, X. Ji, Y.-K. Sun, K. Amine, G. Yushin, L. F. Nazar, J. Cho, P. G. Bruce, *Angew. Rev.* **2012**, *51*, 9994–10024; b) J. Hassoun, S. Panero, P. Reale, B. Scrosati, *Adv. Mater.* **2009**, *21*, 4808–4810; c) J. Hassoun, P. Reale, B. Scrosati, *J. Mater. Chem.* **2007**, *17*, 3668–3677.
[10] C. Xing, M. Zhao, L. Zhao, J. You, X. Cao, Y. Li, *Polym. Chem.* **2013**, *4*, 5726–5734.
[11] M. A. Navarra, J. Manzi L Lombardo, S. Panero, B. Scrosati, *ChemSusChem* **2011**, *4*, 125–130.
[12] Z. He, Q. Cao, B. Jing, X. Wang, Y. Deng, *RSC Adv.* **2017**, *7*, 3240–3248.
[13] a) M. Dahbi, F. Ghamouss, F. Tran-Van, D. Lemordant, M. Anouti, *J. Power Sources* **2011**, *196*, 9743–9750; b) M. Morita, T. Shibata, N. Yoshimoto, M. Ishikawa, *Electrochim. Acta* **2002**, *47*, 2787–2793.
[14] a) L. Larush-Asraf, M. Biton, H. Teller, E. Zinigrad, D. Aurbach, *J. Power Sources* **2007**, *174*, 400–407; b) D. Aurbach, B. Markovsky, G. Salitra, E. Markevich, Y. Talyossef, M. Koltypin, L. Nazar, B. Ellis, D. Kovacheva, *J. Power Sources* **2007**, *165*, 491–499.
[15] a) S. S. Zahng, *J. Power Sources* **2006**, *162*, 1379–1394; b) V. Aravindan, J. Gnanaraj, S. Madhavi, H.-K. Liu, *Chem. Eur. J.* **2011**, *17*, 14326–14346.
[16] X. Kang, S. Zhang, T. R. Jow, W. Xu, C. A. Angell, *Electrochem. Solid-State Lett.* **2002**, *5(1)*, A26–A29.
[17] Z. Chen, W. Q. Lu, J. Liu, K. Amine, *Electrochim. Acta* **2006**, *51*, 3322–3326.
[18] J. Hassoun, M. Wachtler, M. Wohlfahrt-Mehrens, B. Scrosati, *J. Power Sources* **2011**, *2011*, 349–354.
[19] D. Di Lecce, C. Fasciani, B. Scrosati, J. Hassoun, *ACS Appl. Mater. Interfaces* **2015**, *7*, 21198–21207.
[20] L. Long, S. Wang, M. Xiao, Y. Meng, *J. Mater. Chem. A* **2016**, *4*, 10038–10069.
[21] D. L. Wood J Li, C. Daniel, *J. Power Sources* **2015**, *275*, 234–242.
[22] S. Z. Zhang, X. H. Xia, D. Xie, R. C. Xu, Y. J. Xu, Y. Xia, J. B. Wu, Z. J. Yao, X. L. Wang, J. P. Tu, *J. Power Sources* **2019**, *409*, 31–37.
[23] X. Guan, Q. Wu, X. Zhang, X. Guo, C. Li, J. Xu, *Chem. Eng. J.* **2020**, *382*, 122935.
[24] A. Ponrouch, D. Monti, A. Boschin, B. Steen, P. Johansson, M. R. Palacín, *J. Mater. Chem. A* **2015**, *3*, 22–42.
[25] R. D. Simoes, A. E. Job, D. L. Chinaglia, V. Zucolotto, J. C. Camargo-Filho, N. Alves, J. A. Giacometti, O. N. Oliveira, C. J. L. Constantino, *J. Raman Spectrosc.* **2005**, *36*, 1118–1124.
[26] a) E. Zinigrad, L. Larush-Asraf, G. Salitra, M. Sprecher, D. Aurbach, *Thermochim. Acta* **2007**, *457*, 64–69; b) S. Hyoung Oh, T. Yim, E. Pomerantseva, L. F. Nazar, *Electrochem. Solid-State Lett.* **2011**, *14*, A185.
[27] a) R. Chen, L. Zhu, F. Wu, L. Li, R. Zhang, S. Chen, *J. Power Sources* **2014**, *245*, 730–738; b) L. D. Ellis, S. Buteau, S. G. Hames, L. M. Thompson, D. S. Hall, J. R. Dahn, *J. Electrochem. Soc.* **2018**, *165*, A256-A262.
[28] a) A. Jain, J. S. Kumar, S. Srikanth, V. T. Rathod, D. Roy Mahapatra, *Polym. Eng. Sci.* **2013**, *53*, 707–715; b) A. Martinelli, M. A. Navarra, A. Matic, S. Panero, P. Jacobsson, L. Börjesson, B. Scrosati, *Electrochim. Acta* **2005**, *50*, 3992–3997; c) S. M. Lebedev, O. S. Gefle, S. N. Tkachenko, *Russ. Phys. J.* **2011**, *54*, 679–685.
[29] a) F. I. Chowdhury, M. U. Khandaker, Y. M. Amin, M. Z. Kufian, H. J. Woo, *Ionics* **2017**, *23*, 275–284; b) R. Holomb, W. Xu, H. Markusson, P. Johansson, P. Jacobsson, *J. Phys. Chem. A* **2006**, *110*, 11467–11472.
[30] M. Latour, *Ferroelectrics* **2011**, *60*, 71–76.
[31] L. Aguilera, J. Scheersa, A. Matic, *Phys. Chem. Chem. Phys.* **2016**, *18*, 25458–25464.
[32] K. Vignarooban, P. Badami, M. A. K. L. Dissanayake, P. Ravirajan, A. M. Kannan, *Ionics* **2017**, *23*, 2817–2822.
[33] R. Baskaran, S. Selvasekarapandian, G. Hirankumar, M. S. Bhuvaneswari, *J. Power Sources* **2004**, *134*, 235–240.
[34] J. Hassoun, A. Fernicola, M. A. Navarra, S. Panero, B. Scrosati, *J. Power Sources* **2010**, *195*, 574–579.
[35] L. Lombardo, M. A. Navarra, S. Panero, L. A. Medina, A. Matic, J. Hassoun, *J. Power Sources* **2014**, *245*, 232–235.
[36] a) A. Paolone, O. Palumbo, F. Teocoli, R. Cantelli, J. Hassoun, *Solid State Phenom.* **2012**, *184*, 351–354; b) F. Teocoli, A. Paolone, O. Palumbo, M. A. Navarra, M. Casciola, A. Donnadio, *J. Polym. Sci. Part B* **2012**, *50*, 1421–1425; c) R. Cantelli, O. Palumbo, A. Paolone, C. M. Jensen, M. T. Kuba, R. Ayabe, *J. Alloys Compd.* **2007**, *446–447*, 260–263.
[37] J. Hassoun, G. Derrien, S. Panero, B. Scrosati, *Adv. Mater.* **2008**, *20*, 3169–3175.

Manuscript received: April 7, 2020
Revised manuscript received: May 28, 2020
Accepted manuscript online: June 12, 2020
Version of record online: July 13, 2020